

EFFECT OF FREE-EDGES ON MELT POOL GEOMETRY AND SOLIDIFICATION MICROSTRUCTURE IN BEAM-BASED FABRICATION OF BULKY 3-D STRUCTURES

Joy E. Davis and Nathan W. Klingbeil
Department of Mechanical and Materials Engineering
Wright State University
Dayton, OH 45435

Srikanth Bontha
Department of Mechanical Engineering
Temple University
Philadelphia, PA 19122

Abstract

The success of laser and electron beam-based fabrication processes for additive manufacture and repair applications requires the ability to control melt pool geometry while still maintaining a consistent and desirable microstructure. To this end, previous work by the authors has employed point heat source solutions to investigate the effects of process variables (beam power and velocity) on melt pool geometry and solidification microstructure (grain size and morphology) in beam-based fabrication of bulky 3-D structures. However, these results were limited to steady-state conditions away from free-edges. The current work extends the approach to investigate transient behavior in the vicinity of free-edges, and follows the authors' recent work for 2-D thin-wall geometries [1].

Introduction

Both laser and electron beam-based manufacturing are under consideration for aerospace applications, for which the ability to obtain a consistent and desirable microstructure is of critical concern [2–6]. Specific applications for these processes include fabrication of complex parts, addition of features to existing components and repair of damage or defects. While beam-based additive manufacturing offers the promise of increased efficiency and flexibility compared to conventional manufacturing, widespread commercialization of these processes requires the ability to predict and control melt pool size and solidification microstructure. In particular, the mechanical properties of the deposited material are strongly dependent on the solidification microstructure (grain size and morphology), which is controlled by the thermal conditions at the onset of solidification.

The analysis presented herein is based on the 3-D Rosenthal solution for a moving point heat source [7]. The Rosenthal solution was first applied to laser based deposition processes by Dykhuizen and Dobranich [8, 9]. The subsequent identification of dimensionless process variables by Vasinonta *et al.* [10, 11] led to the development of thermal process maps for predicting trends in solidification microstructure by Bontha *et al.* [12–16]. The Rosenthal solution is applicable for semi-infinite geometries, however it does not address the response in the vicinity of a free-edge. Through direct thermal imaging of the melt pool, Rangaswamy *et al.* [17] observed that an increase in melt pool size occurs upon approaching a free-edge, without any change in process variables. Aggarangsi *et al.* [18] developed thermo-mechanical finite element models to understand and control the increase in melt pool size in the vicinity of a free edge. Tan *et al.* [19] have recently used a superposition approach to investigate the transient temperature behavior in

the vicinity of free-edges as a function of dwell time and other process variables. It should finally be noted that nonlinear thermo-mechanical finite element modeling of laser deposition processes has also been used to predict steady-state melt pool behavior and residual stress [10, 11, 20–22], as well as to establish the utility of the Rosenthal solution for predicting trends in solidification microstructure [12–16].

In this work, the effect of free-edges on melt pool geometry and solidification microstructure is investigated for bulky 3-D geometries, and is a direct extension of the authors’ prior work for 2-D thin-wall geometries [1]. Through superposition of the Rosenthal solution, a closed-form solution for the temperature distribution in the vicinity of a free-edge is obtained. Melt pool contours are plotted as a function of distance from the free-edge for both small-scale and large-scale (higher power) processes. In addition, cooling rates and thermal gradients at the onset of solidification are numerically extracted throughout the depth of the melt pool, and are subsequently plotted on solidification maps for predicting trends in grain size and morphology for Ti-6Al-4V. Finally, finite element analysis is performed to verify the validity of the closed-form solution, as well as to investigate solidification behavior when the beam reaches the edge and is turned off.

3-D Rosenthal Solution

This study considers the bulky 3-D geometry of Fig. 1, in which the process variables of interest are the absorbed beam power αQ and velocity V . It is assumed that the height h , length L and width b are sufficiently large such that the steady-state Rosenthal solution for a moving point heat source applies.

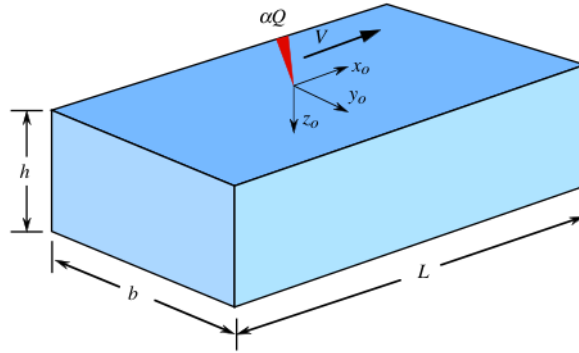


Figure 1: Bulky 3-D Geometry

For the geometry of Fig. 1, the temperature at a point relative to the position of the point heat source has been given in dimensionless form by Vasinonta *et al.* [10, 11] as

$$\bar{T} = \frac{e^{-(\bar{x}_0 + \sqrt{\bar{x}_0^2 + \bar{y}_0^2 + \bar{z}_0^2})}}{2\sqrt{\bar{x}_0^2 + \bar{y}_0^2 + \bar{z}_0^2}}. \quad (1)$$

The dimensionless variables in eq. (1) are defined in terms of the absorbed beam power αQ and velocity V as

$$\bar{T} = \frac{T - T_0}{\left(\frac{\alpha Q}{\pi k}\right) \left(\frac{\rho c V}{2k}\right)}, \quad \bar{x}_0 = \frac{x_0}{\frac{2k}{\rho c V}}, \quad \bar{y}_0 = \frac{y_0}{\frac{2k}{\rho c V}} \quad \text{and} \quad \bar{z}_0 = \frac{z_0}{\frac{2k}{\rho c V}}. \quad (2)$$

In the above normalizations, T is the temperature at a location (x_0, y_0, z_0) relative to the moving point heat source and T_0 is the initial temperature of the substrate. The relative coordinates (x_0, y_0, z_0) are related to fixed spatial coordinates (x, y, z) at any time t as $(x_0, y_0, z_0) = (x - Vt, y, z)$, where V is the velocity of the beam. Also in eq. (4), the thermophysical properties ρ , c and k are the density, specific heat and thermal conductivity of the material, which are assumed to be temperature-independent. In the subsequent sections, results are presented for both small-scale and large-scale processes, which are characterized in terms of the dimensionless melting temperature

$$\bar{T} = \bar{T}_m = \frac{T_m - T_0}{\left(\frac{\alpha Q}{\pi k}\right) \left(\frac{\rho c V}{2k}\right)}. \quad (3)$$

Closed-Form Solution in Vicinity of Free-Edge

For the case of temperature-independent properties, a closed-form solution for the temperature distribution in the vicinity of the free-edge can be modeled by superposition of two point-heat sources approaching one another, with the line of symmetry representing the free-edge. This is because the symmetry condition is equivalent to thermal insulation, which is essentially the case at the free-edge. This of course assumes that convection and radiation are negligible compared to conduction, which is generally well accepted for beam-based deposition processes.

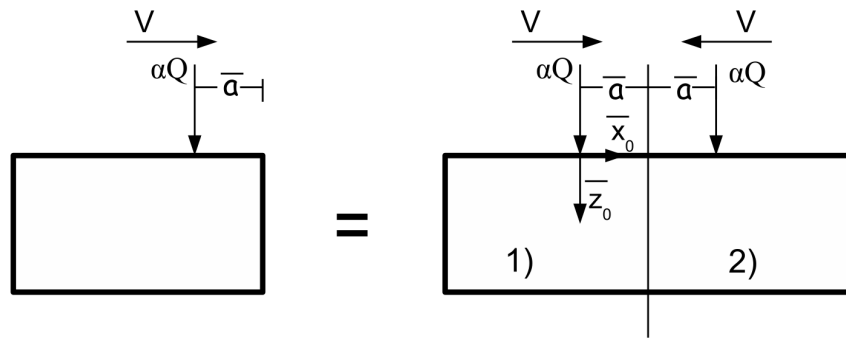


Figure 2: Free-Edge Representation

A schematic of the superposition approach along the mid-plane $\bar{y}_0 = 0$ is shown in Fig. 2. The dimensionless distance from the free-edge is represented by the parameter \bar{a} . The normalized distance \bar{a}/\bar{l} is used to relate the dimensionless Rosenthal melt pool length \bar{l} to the distance from the free-edge, where

$$\bar{l} = \frac{l}{\frac{2k}{\rho c V}} \quad \text{and} \quad \bar{a} = \frac{a}{\frac{2k}{\rho c V}}. \quad (4)$$

It is important to note that \bar{a}/\bar{l} has the same value as a/l , since the nondimensionalization cancels out. As evident from Fig. 2, the effect of the second heat source can be obtained by replacing \bar{x}_0 with the quantity $(2\bar{a}-\bar{x}_0)$ in the Rosenthal solution of eq. (1). Along the mid-plane $\bar{y}_0 = 0$, the total solution for both heat sources (or for a single source approaching the free-edge) is given by superposition as

$$\bar{T} = \frac{e^{-(\bar{x}_0 + \sqrt{\bar{x}_0^2 + \bar{z}_0^2})}}{2\sqrt{\bar{x}_0^2 + \bar{z}_0^2}} + \frac{e^{-((2\bar{a}-\bar{x}_0) + \sqrt{(2\bar{a}-\bar{x}_0)^2 + \bar{z}_0^2})}}{2\sqrt{(2\bar{a}-\bar{x}_0)^2 + \bar{z}_0^2}}. \quad (5)$$

As discussed in [12–16], the microstructure (grain size and morphology) of deposited metals depends on cooling rates and thermal gradients at the onset of solidification (i.e., along the trailing boundary of the melt pool). In the vicinity of the free-edge, expressions for the dimensionless cooling rate and thermal gradient can be obtained through analytical differentiation of eq. (5). As such, the dimensionless cooling rate is given by

$$\begin{aligned} \frac{\partial \bar{T}}{\partial \bar{t}} = & \frac{e^{-\{(\bar{x}-\bar{t}) + \sqrt{(\bar{x}-\bar{t})^2 + \bar{z}_0^2}\}}}{2\sqrt{(\bar{x}-\bar{t})^2 + \bar{z}_0^2}} \left\{ 1 + \frac{(\bar{x}-\bar{t})}{\left(\sqrt{(\bar{x}-\bar{t})^2 + \bar{z}_0^2}\right)} + \frac{(\bar{x}-\bar{t})}{\left((\bar{x}-\bar{t})^2 + \bar{z}_0^2\right)} \right\} \\ & + \frac{e^{-\{((2\bar{a}-\bar{x})-\bar{t}) + \sqrt{((2\bar{a}-\bar{x})-\bar{t})^2 + \bar{z}_0^2}\}}}{2\sqrt{((2\bar{a}-\bar{x})-\bar{t})^2 + \bar{z}_0^2}} \left\{ 1 + \frac{((2\bar{a}-\bar{x})-\bar{t})}{\left(\sqrt{((2\bar{a}-\bar{x})-\bar{t})^2 + \bar{z}_0^2}\right)} + \frac{((2\bar{a}-\bar{x})-\bar{t})}{\left(((2\bar{a}-\bar{x})-\bar{t})^2 + \bar{z}_0^2\right)} \right\}. \end{aligned} \quad (6)$$

In eq. (6), the dimensionless variable \bar{x} is related to the relative coordinate \bar{x}_0 by the relationship

$\bar{x} = \bar{x}_0 + \bar{t}$, where the dimensionless time \bar{t} is defined as $\bar{t} = \frac{t}{2k/\rho c V^2}$. The dimensionless thermal gradient is given by

$$\nabla \bar{T} = \sqrt{\left(\frac{\partial \bar{T}}{\partial \bar{x}_0}\right)^2 + \left(\frac{\partial \bar{T}}{\partial \bar{z}_0}\right)^2}, \quad (7)$$

where $\frac{\partial \bar{T}}{\partial \bar{x}_0}$ and $\frac{\partial \bar{T}}{\partial \bar{z}_0}$ are obtained by differentiating eq. (5) and are given in [23].

As discussed in [15, 16], the dimensionless cooling rate and thermal gradient are related to their actual values as

$$\frac{\partial \bar{T}}{\partial \bar{t}} = \left(\frac{2k}{\rho c V} \right)^2 \left(\frac{\pi k}{\alpha Q V} \right) \frac{\partial T}{\partial t} \quad (8)$$

and

$$|\bar{\nabla T}| = \left(\frac{2k}{\rho c V} \right)^2 \left(\frac{\pi k}{\alpha Q} \right) |\nabla T|. \quad (9)$$

Representative Results for Bulky 3-D Geometry

This section includes representative dimensionless results which illustrate the effect of the free-edge on melt pool geometry and solidification microstructure for both small-scale and large-scale processes. For each case, the melt pool geometry is plotted a function of distance from the free-edge. In addition, the dimensionless cooling rate and thermal gradient are numerically extracted and evaluated along the trailing edge of the melt pool. Results are subsequently plotted on solidification maps for Ti-6Al-4V. In so doing, the thermophysical properties are assumed constant at the melting temperature $T_m = 1654^\circ\text{C}$, while the absorption coefficient is assumed to be $\alpha = 0.35$. Finally, the velocity is held constant at $V = 8.47 \text{ mm/s}$. The above values are in keeping with those used in the authors' prior work [1, 6, 12–16].

Effect of Free-Edge for Small-Scale Processes

Dimensionless melt pool geometries are shown in Fig. 3 for the case of $\bar{T}_m = 2.88$. With the parameters specified above, this corresponds to a beam power of $Q = 325 \text{ W}$. The steady-state Rosenthal melt pool is seen on the far left. The melt pool is an almost circular cross section and increases in size as the point heat source approaches the free-edge.

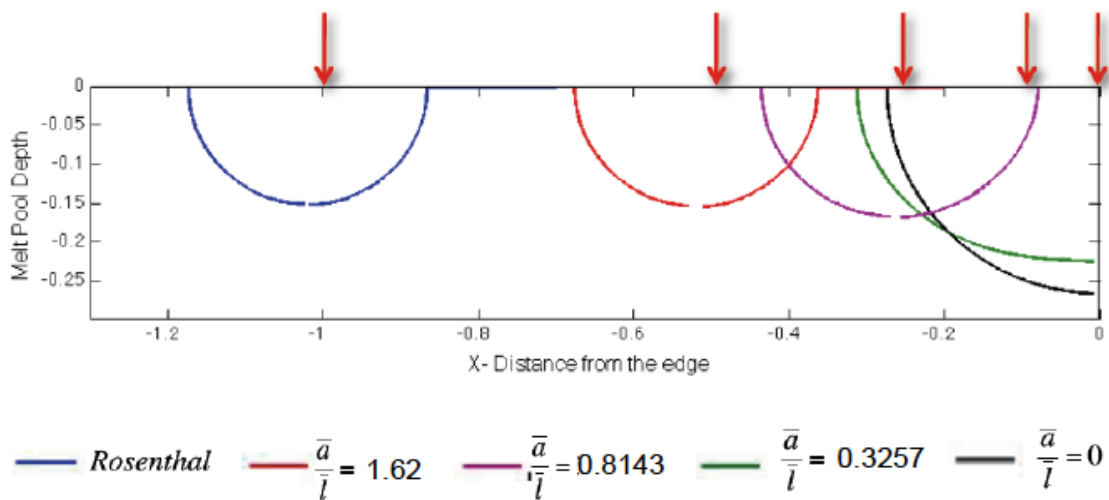
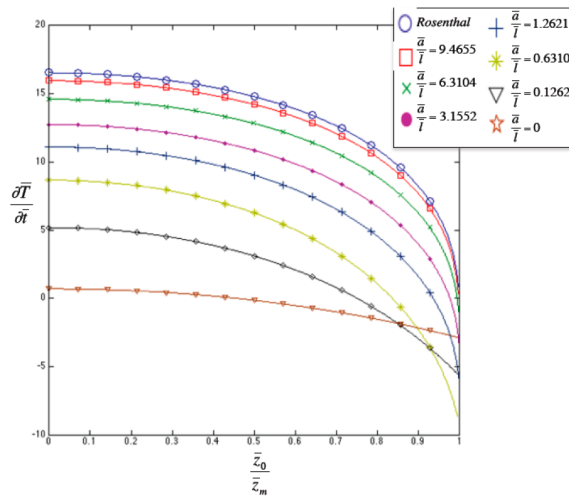
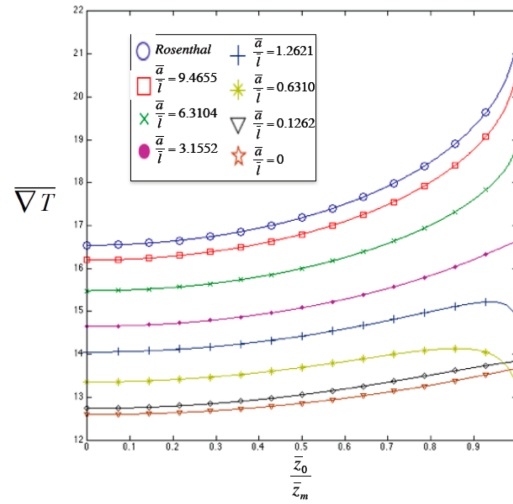


Figure 3: Small-Scale Process Melt Pool Geometry, $\bar{T}_m = 2.88$



(a) Small-Scale Process Cooling Rate



(b) Small-Scale Process Thermal Gradient

Figure 4: Small-Scale (a) Cooling Rate and (b) Thermal Gradient

Representative results for the dimensionless cooling rate are plotted in Fig. 4 (a) as a function of relative depth within the melt pool for selected values of \bar{a}/\bar{l} . The relative depth within the melt pool varies in the range $0 \leq \bar{z}_0/\bar{z}_m \leq 1$, where \bar{z}_m is the maximum depth of the melt pool for the given value of \bar{T}_m . As seen in the figure, the cooling rate decreases (and ultimately becomes negative) as the point heat source approaches the edge. This is in keeping with the increase in melt pool size illustrated in Fig. 3, which is somewhat analogous to an increase in incident energy. The negative cooling rate signifies heating (as opposed to cooling) of the melt pool boundary, as there is nowhere for the heat to go at the free-edge. Representative results for the dimensionless thermal gradient are shown in Fig. 4 (b). The thermal gradient decreases as the beam approaches the free edge, which is again analogous to an increase in incident energy. However, the thermal gradient appears to be somewhat less sensitive to the free edge than the cooling rate, particularly near the surface of the deposit.

Effect of Free-Edge for Large-Scale Processes

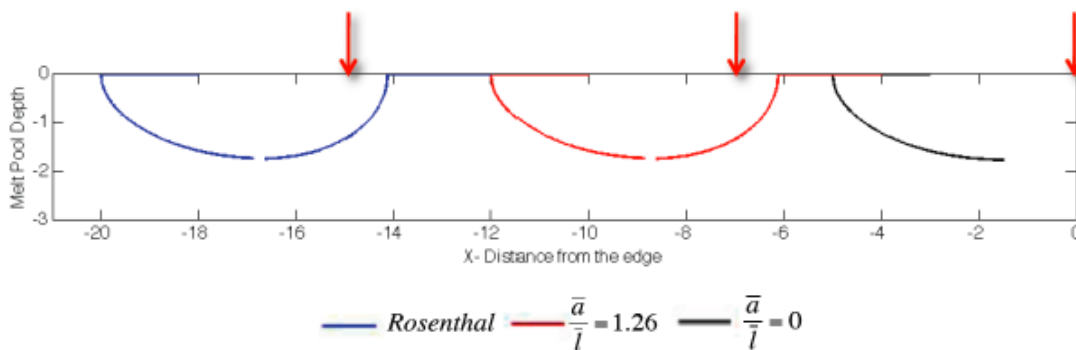
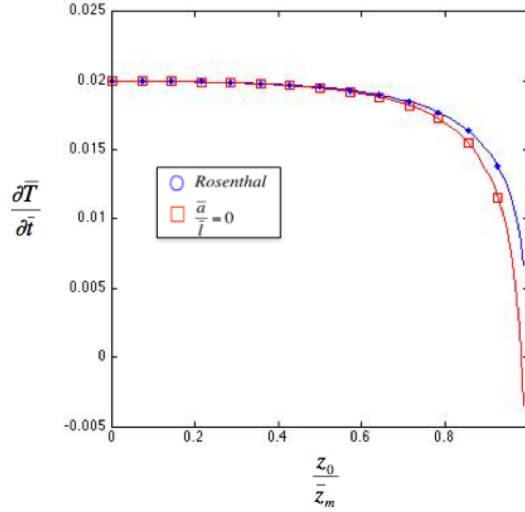
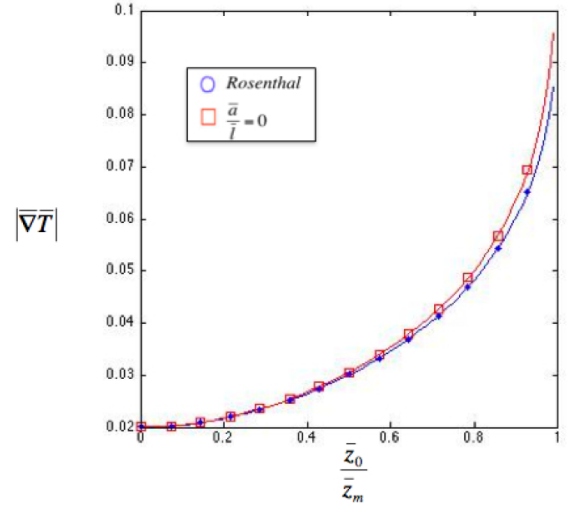


Figure 5: Large-Scale Melt Pool Geometry, $\bar{T}_m = 0.1$



(a) Large-Scale Process Cooling Rate



(b) Large-Scale Process Thermal Gradient

Figure 6: Large-Scale (a) Cooling Rate and (b) Thermal Gradient

Dimensionless melt pool geometries are shown in Fig. 5 for the case of $\bar{T}_m = 0.1$. With the parameters previously specified, this corresponds to a beam power of $Q = 9332 \text{ W}$, which is within the range of high powers used in large-scale processes. Compared to the near-circular cross sections of the small-scale melt pools, the large-scale melt pools have an elongated, surf board-type shape. As the melt pool approaches the free-edge the size does not observably change. This is because the trailing edge of the melt pool is so far away from the free-edge that the insulated condition has little effect on the overall melt pool geometry. The dimensionless cooling rate and thermal gradient for the large-scale process can be seen in Fig. 6. As shown in the figure, both the cooling rate and thermal gradient are insensitive to the beam approaching the free-edge, which is consistent with the negligible change in melt pool geometries shown in Fig. 5.

Finite Element Analysis

Finite element analysis has been used to include the nonlinear effects of temperature-dependent properties and latent heat, as well as to investigate the solidification behavior when the beam reaches the free-edge and is subsequently turned off. In order to reduce computation time, a 2-D axisymmetric finite element model is used instead of a 3-D finite element model. The axisymmetric modeling approach used herein is similar to that used for bulky 3-D geometries by Birnbaum *et al.* [24] and Aggarangsi *et al.* [25]. A representative mesh is shown in Fig. 7, and follows procedures outlined in [15]. The axisymmetric axis is the axis parallel to the direction of the moving point heat source, so that the cylindrical coordinates (z, r) in Fig. 7 correspond to the Cartesian coordinates (x_0, z_0) in Fig. 1. In the axisymmetric model, the point heat source is modeled as moving through the center of a large solid that is twice the geometry actually shown. This is because the top surface of the bulky 3-D geometry is insulated, which is equivalent to a symmetry condition at $\bar{z} = 0$. Therefore the laser power must be twice the actual for the 3-D geometry being modeled. In order to accomplish this $\alpha=0.7$ is used instead of $\alpha=0.35$. This model allows for higher mesh resolution and shorter computation time, with no additional error.

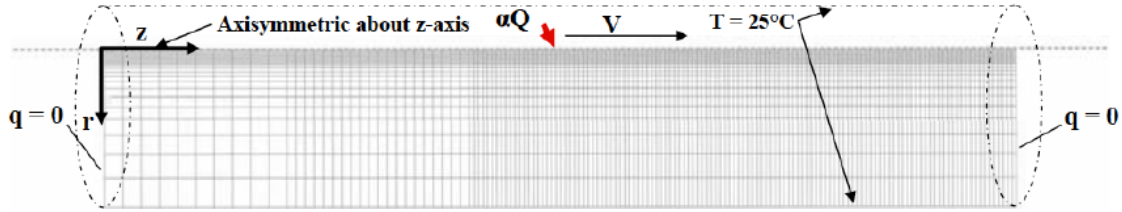


Figure 7: Representative 2-D Axisymmetric Finite Element Mesh for Transient Analysis

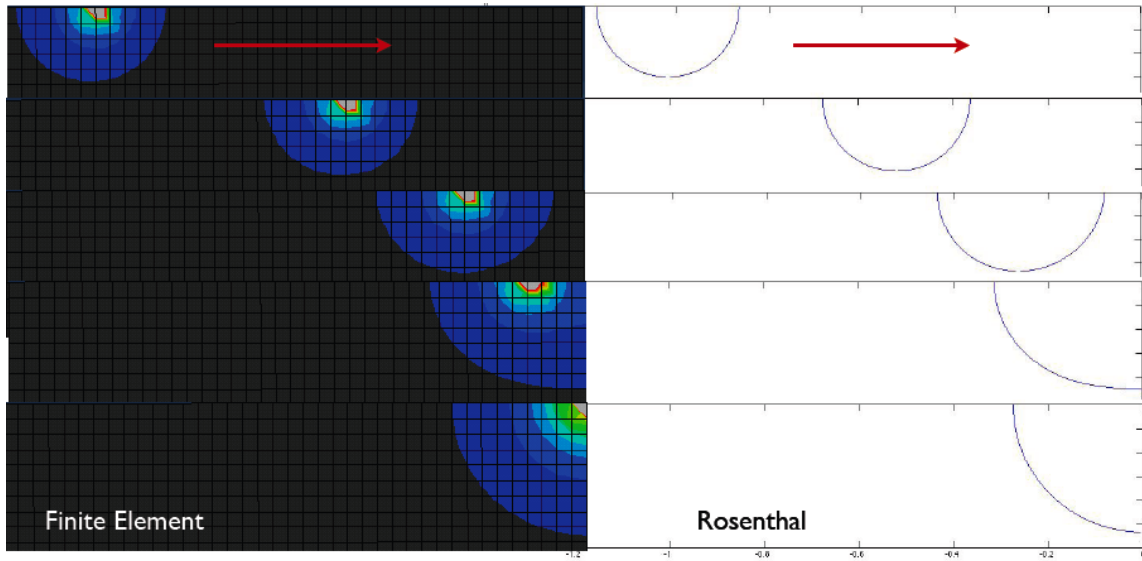


Figure 8: Melt Pool Contours Approaching Free-Edge

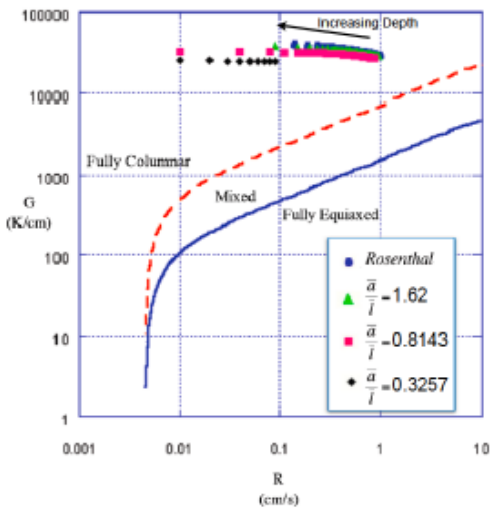
Representative melt pool contours are shown for the case of $\bar{T}_m = 2.88$ in Fig. 8. The results from the finite element analysis (left) compare well with results from the closed-form solution (right), which are also shown in Fig. 3.

Effect of Free-Edge on Grain Morphology

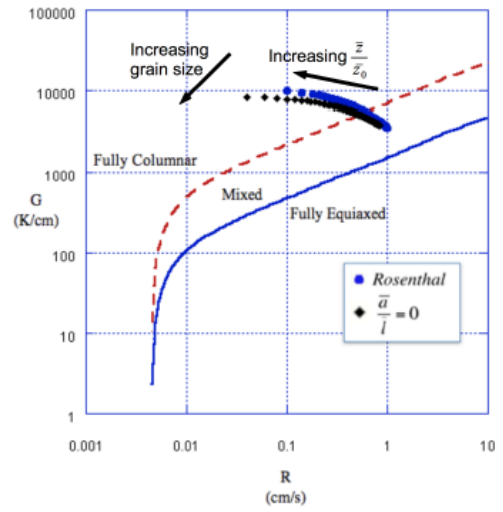
As discussed in [1, 12–16, 26], results for solidification thermal gradient and cooling rate can be interpreted in the context of a solidification map to provide predictions of grain size and morphology in Ti-6Al-4V. Given the solidification cooling rate $\frac{\partial T}{\partial t}$ and thermal gradient $G = |\nabla T|$, the solidification rate R is determined as

$$R = \frac{1}{G} \frac{\partial T}{\partial t}. \quad (10)$$

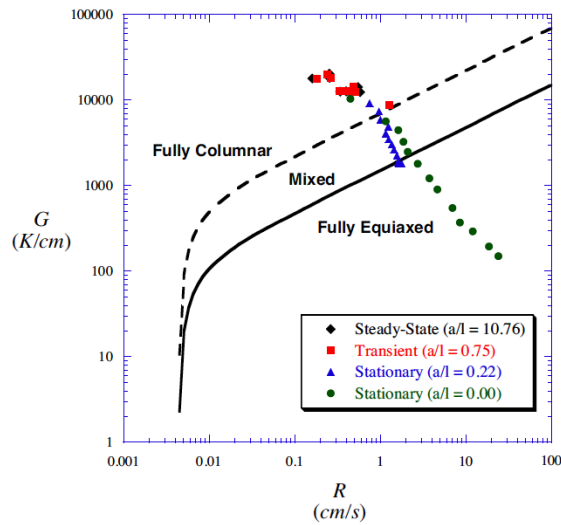
The expected grain morphology can be predicted as either equiaxed, columnar or mixed by plotting points in G vs. R space (i.e., on the “solidification map”), which has been previously calibrated for Ti-6Al-4V [26].



(a) Small-Scale Solidification Map, $\bar{T}_m = 2.88$



(b) Large-Scale Solidification Map, $\bar{T}_m = 0.1$



(c) Small-Scale FEA Results, $\bar{T}_m = 2.88$

Figure 9: Solidification Maps for (a) Small-Scale Processes (b) Large-Scale Processes and (c) Small-Scale Finite Element Results

Solidification maps showing the effect of free-edges on predicted grain morphology for both small-scale and large-scale deposition of bulky Ti-6Al-4V deposits are shown in Fig. 9. The values of G and R plotted in Fig. 9 (a) and (b) are extracted from the dimensionless cooling rate and thermal gradient plots of Figs. 4 and 6, with thermophysical properties at 1654°C and process variables as previously noted. The values of G and R plotted in Fig. 9 (c) are extracted directly from the finite element analysis, with temperature-dependent properties for Ti-6Al-4V.

For the small-scale process of Fig.9 (a), the microstructure remains in the fully columnar region as the free-edge is approached. However, the free-edge acts to decrease both the solidification rate

and thermal gradient, which causes an increase in grain size. So as the free-edge is approached, results suggest a trend toward columnar grains of increasing size.

For the large-scale process of Fig. 9 (b), there is very little change in solidification microstructure as the beam approaches the free-edge. This is expected based on the results of Fig. 6. For all distances from the free-edge there is a grading of the microstructure throughout the depth of the deposit, with a transition from columnar to mixed/equiaxed microstructure at the surface. This is in keeping with results of the authors' prior work [16].

From the small-scale finite element results of Fig. 9 (c), it is clear that the data points from both the steady-state and transient melt pools fall in the fully columnar region, which is in keeping with the results of Fig. 9 (a). However, results also suggest that a transition to equiaxed microstructure can occur when the beam is turned off at the free-edge (stationary melt pool). Results not shown here reveal a similar effect when the beam returns from the free-edge [23]. Thus, even for small-scale processes, the potential for an equiaxed microstructure exists right *at* the free-edge.

Summary and Conclusions

This study has considered the effect of free-edges on solidification microstructure (grain size and morphology) in beam-based fabrication of bulky 3-D structures. Based on superposition of the steady-state Rosenthal solution for a moving point heat source, a closed-form solution has been presented for the thermal history in the vicinity of a free-edge. Dimensionless cooling rates and thermal gradients have been extracted from the closed-form solution and plotted as a function of normalized distance from the free-edge, for both small-scale and large-scale processes. In addition, finite element analysis has been used to include the nonlinear effects of temperature-dependent properties and latent heat, as well as to investigate stationary melt pool behavior when the beam is turned off at the free-edge. Results from both the closed-form and FEA solutions have been plotted on solidification maps for predicting grain size and morphology in Ti-6Al-4V. For small-scale processes, results suggest that melt pool geometry may be more sensitive to free-edges than the solidification microstructure. This suggests that the control of melt pool size may be possible without affecting microstructure, which is an important result for process developers. Results further suggest that for large-scale processes, both melt pool geometry and microstructure are insensitive to the beam *approaching* free-edges. Finally, results suggest that a substantial free-edge effect is possible at the very end of a pass, when the beam either returns from the free-edge or is shut off. In particular, results suggest that even for small-scale processes, a transition to equiaxed microstructure is possible at free-edges.

Acknowledgments

This work has been supported by the National Science Foundation, grant numbers DMI-0224517 and CMMI-0700509, by the joint AFRL/DAGSI Research Program, project number ML-WSU-01-11, and by Wright State University and the Ohio Board of Regents. Any opinions or findings contained herein are those of the authors, and do not necessarily reflect the views of the National Science Foundation, the Ohio Board of Regents or Wright State University.

References

- [1] J. Davis, N. Klingbeil, and S. Bontha, "Effect of Free-Edges on Melt Pool Geometry and Solidification Microstructure in Beam-Based Fabrication of Thin-Wall Structures," in *Solid Freeform Fabrication Proceedings*, (Austin, TX), August 2009.
- [2] P. Kobryn, E. Moore, and S. Semiatin, "The Effect of Laser Power and Traverse Speed on Microstructure, Porosity, and Build Height in Laser Deposited Ti-6Al-4V," *Scripta Materialia*, vol. 43, pp. 299–305, 2000.
- [3] F. Arcella and F. Froes, "Producing Titanium Aerospace Components from Powder Using Laser Forming," *JOM*, vol. 52, pp. 28–30, May 2000.
- [4] P. Kobryn and S. Semiatin, "The Laser Additive Manufacture of Ti-6Al-4V," *JOM*, vol. 53, no. 9, pp. 40–42, 2001.
- [5] J. Beuth and N. Klingbeil, "The Role of Process Variables in Laser-Based Direct Metal Solid Freeform Fabrication," *JOM*, pp. 36–39, September 2001.
- [6] N.W.Klingbeil, C. Brown, S. Bontha, P. Kobryn, and H. Fraser, "Prediction of Microstructure in Laser Deposition of Titanium Alloys," in *Solid Freeform Fabrication Proceedings*, (Austin, TX), pp. 142–149, August 2002.
- [7] D. Rosenthal, "The Theory of Moving Sources of Heat and Its Applications to Metal Treatments," *Transactions of ASME*, vol. 68, pp. 849–866, 1946.
- [8] R. Dykhuizen and D. Dobranich, "Cooling Rates in the LENS Process," *Sandia National Laboratories Internal Report*, 1998.
- [9] R. Dykhuizen and D. Dobranich, "Analytical Thermal Models for the LENS Process," *Sandia National Laboratories Internal Report*, 1998.
- [10] A. Vasinonta, J. Beuth, and M. Griffith, "Process Maps for Controlling Residual Stress and Melt Pool Size in Laser-Based SFF Processes," in *Solid Freeform Fabrication Proceedings*, (Austin, TX), pp. 200–208, August 2000.
- [11] A. Vasinonta, J. Beuth, and M. Griffith, "A Process Map for Consistent Build Conditions in the Solid Freeform Fabrication of Thin-Walled Structures," *ASME Journal of Manufacturing Science and Engineering*, vol. 123, pp. 615–622, 2001.
- [12] S. Bontha and N. Klingbeil, "Thermal Process Maps for Controlling Microstructure in Laser-Based Solid Freeform Fabrication," in *Solid Freeform Fabrication Proceedings*, (Austin, TX), pp. 219–226, August 2003.
- [13] N. Klingbeil, S. Bontha, C. Brown, D. Gaddam, P. Kobryn, H. Fraser, and J. Sears, "Effects of Process Variables and Size Scale on Solidification Microstructure in Laser-Based Solid Freeform Fabrication of Ti-6Al-4V," in *Solid Freeform Fabrication Proceedings*, (Austin, TX), August 2004.

- [14] S. Bontha, N. Klingbeil, P. Kobryn, and H. Fraser, "Thermal Process Maps for Predicting Solidification Microstructure in Laser Fabrication of Thin Wall Structures," *Journal of Materials Processing Technology*, vol. 178, no. 1-3, pp. 135–142, 2006.
- [15] S. Bontha, *The Effect of Process Variables on Microstructure in Laser Deposited Materials*. PhD thesis, Wright State University, 2006.
- [16] S. Bontha, N. Klingbeil, P. Kobryn, and H. L. Fraser, "Effects of Process Variables and Size Scale on Solidification Microstructure in Beam-Based Fabrication of Bulky 3D Structures," *Materials Science and Engineering A*, vol. 513-514, pp. 311–318, 2009.
- [17] P. Rangaswamy, T. Holden, R. Rogge, and M. Griffith, "Residual Stresses in Components Formed by the Laser Engineered Net Shaping (LENS) Process," *Journal of Strain Analysis for Engineering Design*, vol. 38, pp. 519–527, November 2003.
- [18] P. Aggarangsi, J. Beuth, and M. Griffith, "Melt Pool Size and Stress Control for Laser-Based Deposition Near a Free Edge," in *Solid Freeform Fabrication Proceedings*, (Austin, TX), pp. 196–207, Solid Freeform Fabrication Symposium, August 2003.
- [19] H. Tan, J. Chen, E. Zhang, X. Lin, and W. Huang, "Process Analysis for Laser Solid Forming of Thin-Wall Structure," *International Journal of Machine Tools and Manufacture*, vol. 50, pp. 1–8, January 2010.
- [20] A. Vasinonta, *Process Maps for Melt Pool Size and Residual Stress in Laser-Based Solid Freeform Fabrication*. PhD thesis, Carnegie Mellon University, May 2002.
- [21] A. Vasinonta, J. Beuth, and M. Griffith, "Process Maps for Laser Deposition of Thin-Walled Structures," in *Solid Freeform Fabrication Proceedings*, (Austin, TX), pp. 383–391, August 1999.
- [22] K. Dai and L. Shaw, "Thermal and Stress Modeling of Multi-Material Laser Processing," *Acta Materialia*, vol. 49, pp. 4171–4181, 2001.
- [23] J. E. Davis, "Effect of Free-Edges on Melt Pool Geometry and Solidification Microstructure in Beam-Based Fabrication Methods," Master's thesis, Wright State University, 2010.
- [24] A. Birnbaum, J. Beuth, and J. Sears, "Scaling Effects in Laser-Based Additive Manufacturing Processes," in *Solid Freeform Fabrication Proceedings*, (Austin, TX), August 2004.
- [25] P. Aggarangsi, J. Beuth, and D. Gill, "Transient Changes in Melt Pool Size in Laser Additive Manufacturing Processes," in *Solid Freeform Fabrication Proceedings*, (Austin, TX), August 2004.
- [26] P. Kobryn and S. Semiatin, "Microstructure and Texture Evolution during Solidification Processing of Ti-6Al-4V," *Journal of Materials Processing Technology*, vol. 135, pp. 330–339, 2003.